Research article

JGS
Journal of the Geological Society

https://doi.org/10.1144/jgs2024-228 | Vol. 182 | 2025 | jgs2024-228

The combined role of near-bed currents and sub-seafloor processes in the transport and pervasive burial of microplastics in submarine canyons

Ed Keavney[1]*, Ian A. Kane[2], Michael A. Clare[3], David M. Hodgson[1], Veerle A. I. Huvenne[3], Esther J. Sumner[4], Jeff Peakall[1], Furu Mienis[5] and Jonathan Kranenburg[5]

[1] School of Earth and Environment, University of Leeds, Leeds LS2 9JT, UK
[2] Department of Earth and Environmental Science, University of Manchester, Manchester M13 9Pl, UK
[3] Ocean BioGeosciences, National Oceanography Centre, Southampton SO14 3ZH, UK
[4] School of Ocean and Earth Science, University of Southampton, Southampton SO14 3ZH, UK
[5] Department of Ocean Systems, Royal Netherlands Institute for Sea Research (NIOZ-Texel), Den Burg, The Netherlands
EK, 0000-0002-2390-3339; IAK, 0000-0002-0371-4223; MAC, 0000-0003-1448-3878; DMH, 0000-0003-3711-635X; VAIH, 0000-0001-7135-6360; EJS, 0000-0002-3394-1670; JP, 0000-0003-3382-4578; FM, 0000-0002-7370-0652
* Correspondence: ed.keavney@gmail.com

Abstract: Submarine canyons are important conduits for microplastic transport to the deep sea, but the processes involved in that transport and how faithfully seafloor deposits record trends in pollution remain unclear. We use sediment push cores for microplastic and sediment grain-size analysis from two transects across the Whittard Canyon, UK, to investigate the roles of near-bed flows and sub-seafloor processes in the transport and burial of microplastics and semi-synthetic microfibres. Microplastic and microfibre pollution is pervasive across the canyon at both transects, from the thalweg and from 500 m higher on the flanks, despite turbidity currents being confined to the canyon thalweg. We calculate sediment accumulation rates from ^{210}Pb dating and show that microplastic concentrations remain similar at sediment depths down to 10 cm. Throughout the Whittard Canyon there is an observed uniformity in the gradual decline in microfibre concentration with sediment depth, despite the variable sample locations and marked variations in sediment accumulation rates. Furthermore, the huge global increase in plastic production rates over time is not recorded, and microplastics are present in sediments that predate the mass production of plastic. The interaction of turbidity currents, deep tidally driven currents and sub-seafloor processes affects microfibre burial processes in the deep sea and shreds any potential signal that microplastics may provide as indicators of historical plastic production rates; complicating the use of microplastics as fully reliable markers of Anthropocene onset.

Supplementary material: The Supplementary material includes an extended 'Setting and methods', and the data tables for the grain-size/microplastic analysis, contamination control measures, micro-Fourier transform infrared (μ-FTIR) spectroscopy, and ^{210}Pb sediment accumulation rate analysis, and is available at https://doi.org/10.6084/m9.figshare.c.7803458

Received 21 October 2024; **revised** 1 May 2025; **accepted** 1 May 2025

Plastic production has increased by 700%, from 50 million tonnes (Mt) in the 1970s to more than 400 Mt in 2022 (Plastics Europe 2023). More than 10 Mt of plastic enters the world's ocean annually (Lebreton *et al.* 2017). Microplastics (<1 mm diameter particles) represent *c.* 13.5% of the marine plastic budget (Koelmans *et al.* 2017), including primary (manufactured particles: Zitko and Hanlon 1991) and secondary (derived from the breakdown of macroplastics: Andrady 2011) microplastics. Semi-synthetic microfibres (e.g. composed of rayon and chlorinated rubber) are also persistent in the natural environment (Athey and Erdle 2022; Finnegan *et al.* 2022), are observed in deep-sea sediments (Woodall *et al.* 2014) and have similar detrimental effects on biota (Jiang *et al.* 2024) as plastic microfibres. Semi-synthetic microfibres are commonly used in clothes manufacturing (e.g. Napper and Thompson 2016) and cigarette filters (e.g. Belzagui *et al.* 2021). Therefore, we use 'microfibre' to encompass synthetic and semi-synthetic microfibres, and 'anthropogenic microparticles' to encompass both microplastic particles and microfibres.

Lacustrine and shallow-marine settings act as archives to calculate the rate and quantity of pollutant delivery (such as anthropogenic microparticles) and allow monitoring of how stresses on ecosystems change over time (Brandon *et al.* 2019; Uddin *et al.* 2021 and references therein). Few studies have acquired sedimentary time-series records of anthropogenic microparticles in the deep sea (e.g. Chen *et al.* 2020), despite it being the ultimate sink for plastics (Thompson *et al.* 2004; Woodall *et al.* 2014; Koelmans *et al.* 2017; Choy *et al.* 2019). Furthermore, none exist for submarine canyons, the main conduits for delivering particulate matter (Normark 1970; Talling *et al.* 2023), including pollutants (Paull *et al.* 2002; Zhong and Peng 2021; Pierdomenico *et al.* 2023) from terrestrial and coastal settings to the deep sea, and hosts to important seafloor ecosystems (Treignier *et al.* 2006; Fernandez-Arcaya *et al.* 2017). Avalanches of sediment, known as turbidity currents, flow through submarine canyons and are responsible for generating Earth's largest sediment accumulations (Curray and Moore 1971). These flows are thought to be the main agent for anthropogenic microparticle transfer to, and sequestration on, the deep seafloor (Kane and Clare 2019; Pohl *et al.* 2020; Rohais *et al.* 2024; Zhang *et al.* 2024; Chen *et al.* 2025). However, it is increasingly recognized that other hydrodynamic processes can also affect anthropogenic microparticle concentrations in the deep sea (e.g. Kane *et al.* 2020), as well as the transport and burial of particulate matter in submarine canyons (e.g. Maier *et al.* 2019; Bailey *et al.* 2024; Hage *et al.* 2024; Palanques *et al.* 2024). It is possible that the importance of these processes has been underestimated and, therefore, that the role of hydrodynamic and sub-

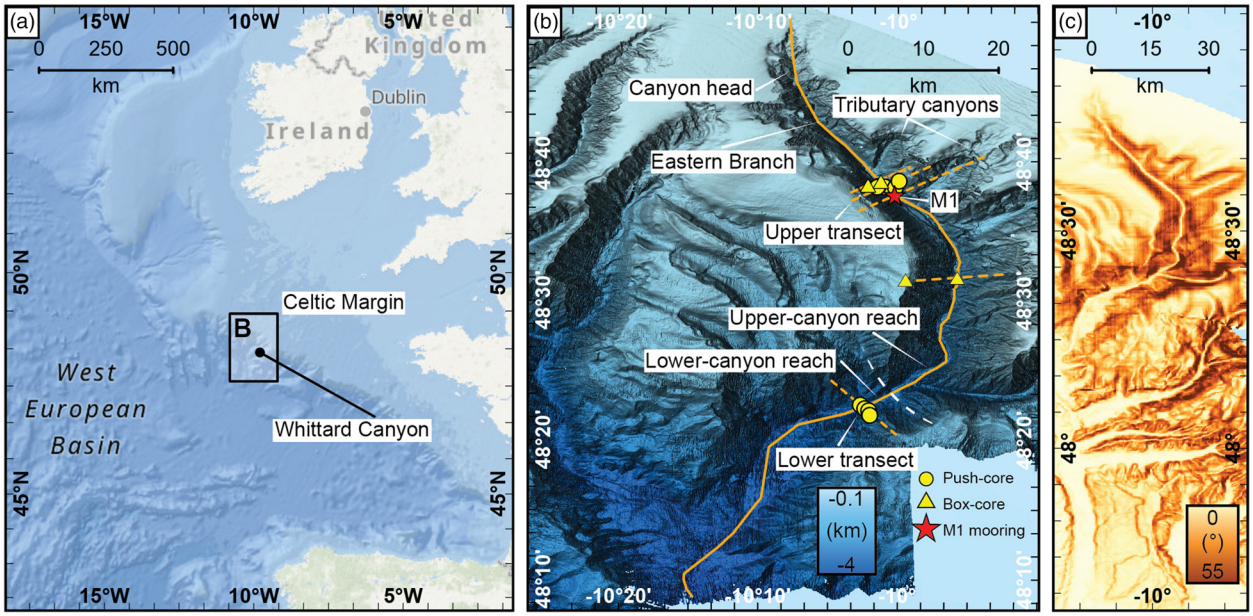

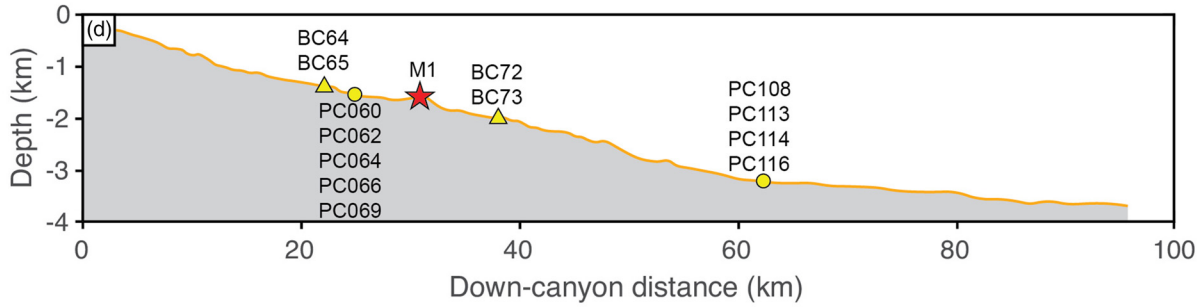

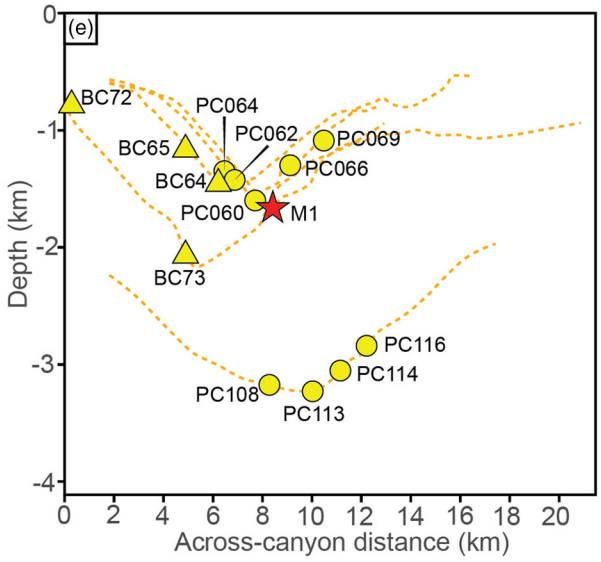

Upper-canyon reach

Push-core	Height above thalweg (m)	Water depth (m)
064	277	1303
062	220	1360
060	34	1546
066	321	1259
069	518	1062

Box-core	Height above thalweg (m)	Water depth (m)
BC64	0	1389
BC65	284	1105
BC72	601	788
BC73	0	2011

Mooring	Height above thalweg (m)	Water depth (m)
M1	30	1500

Lower-canyon reach

Push-core	Height above thalweg (m)	Water depth (m)
108	52	3152
113	0	3204
114	209	2995
116	431	2773

Fig. 1. Location of the data used in this study. (**a**) The location of the Whittard Canyon. (**b**) The locations of the cores and hydrodynamic mooring (M1) in the Eastern Branch of the Whittard Canyon. (**c**) Slope angle map of the Eastern Branch. (**d**) Longitudinal profile of the canyon thalweg. (**e**) Cross-sections through each transect (the locations are shown in b).

seafloor processes, and human activities on anthropogenic microparticle dispersal and burial in submarine canyons, remains unconstrained. Here, we consider the sub-seafloor as the tens of centimetres below the seafloor sediments. This uncertainty results from a lack of targeted seafloor sampling and sedimentological context, therefore limiting our understanding of anthropogenic microparticle fluxes to the deep sea, threats to deep-seafloor ecosystems and deep-sea anthropogenic sedimentary archives.

In addition to anthropogenic microparticle transport via turbidity currents, we hypothesize that other hydrodynamic (e.g. internal tides), anthropogenic (e.g. seabed trawling) and biological (e.g. bioturbation) processes work to (re-)distribute and bury pollutants

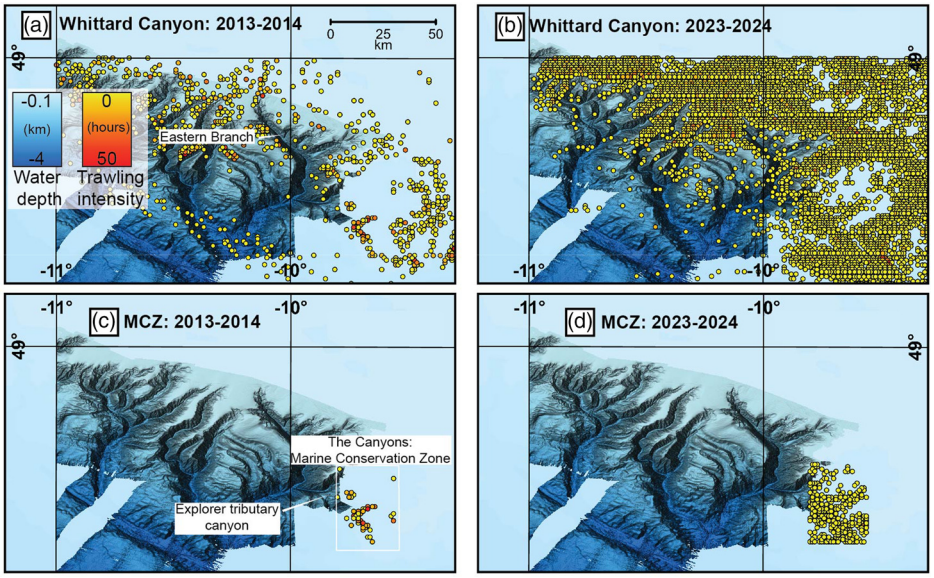

Fig. 2. Intensity of apparent trawling as recorded by Global Fishing Watch. (**a**) The Whittard Canyon 2013–14. (**b**) The Whittard Canyon 2023–24. (**c**) Marine Conservation Zone (MCZ) 2013–14. (**d**) Marine Conservation Zone (2023–24).

across wide areas in submarine canyon systems. We aim to tie anthropogenic microparticle distribution with concepts of deep-water process sedimentology to determine the interplay of anthropogenic microparticle transport and burial processes in the deep sea using a targeted seafloor sampling dataset from two transects across the Whittard Canyon. We assess these process interactions by integrating detailed seafloor observations from multibeam bathymetric mapping and video footage acquired from a remotely operated vehicle (ROV), with analysis of near-seafloor sediments sampled at four box-core locations to quantify sediment accumulation rates, and at nine precisely-located ROV push-core locations to quantify the sediment grain size and anthropogenic microparticle concentration in seafloor sediments. To test the hypothesis, and meet this aim, the following objectives are addressed: (i) to map the distribution and concentration of anthropogenic microparticles throughout a branch of the Whittard Canyon; (ii) to document changes in the anthropogenic micro-particle concentration with burial depth; (iii) to assess sediment grain-size trends associated with the anthropogenic microparticle distribution and concentration, and integrate the findings with sediment accumulation rates; and (iv) to discuss how anthropogenic microparticle transport and burial processes controls their transfer in submarine canyons.

Setting and methods

Whittard Canyon

The head of the Whittard Canyon lies at *c*. 200 m water depth in the Celtic Sea, NE Atlantic, *c*. 300 km from the nearest coast (Fig. 1a). Four main tributary branches incise steeply into the shelf break. The canyon extends oceanwards for *c*. 150 km to *c*. 3800 m water depth (Amaro *et al.* 2016). The upper-canyon reach of the Eastern Branch extends *c*. 55 km, from the head to *c*. 2960 m water depth, with steep canyon flanks and a >2° thalweg slope, with a vertical relief from flank to thalweg of *c*. 1000 m (Fig. 1b, c, e). The lower-canyon reach extends to *c*. 3800 m water depth, with lower gradient canyon flanks and a <2° thalweg slope, with a vertical relief from flank to thalweg of *c*. 1250 m (Fig. 1b, c, e). Further details of the canyon's geomorphology and bathymetry are included in the Supplementary material.

Fishing activity on the Celtic Margin

Fishing activities that disturb the seafloor (i.e. benthic trawling) are common around the head of the Whittard Canyon and on many of its interfluves (Fig. 2). Bottom trawling activity can be a source of marine pollutants (Xue *et al.* 2020) and causes sediment resuspension (Daly *et al.* 2018); however, whether this is explicitly bottom trawling or mid-water trawls in the Whittard Canyon cannot be determined from the Global Fishing Watch (2024) data (see Supplementary Material). The cumulative, annual apparent trawling effort for 2013–14 and 2023–24 was exported from Global Fishing Watch (2024) for an area of 16 650 km^2 (48–49° N, 9–11° W) around the continental shelf and the Whittard Canyon (Fig. 2a, b). The apparent trawling effort for the same period for the 661 km^2 (48° 10′ 2.56″–48° 29′ 59.74″ N, 9° 33′ 34.59″–9° 47′ 52.25″ W) area covered by The Canyons Marine Conservation Zone (MCZ) was also exported (Fig. 2c, d). The MCZ was designated in November 2013 for the features 'Cold-water coral reef' and 'Deep seabed', following identification of vulnerable ecosystems in the area (Davies *et al.* 2014). Later on, two further features were added to the site designation: 'Coral gardens' and 'Sea-pen and burrowing megafauna communities'. The intensity of apparent trawling on the Celtic Margin increased five-fold in the 10 year period from 2013–14 to 2023–24 (Global Fishing Watch 2024) (Fig. 2), but was banned in the majority of The Canyons MCZ in June 2022 as new fisheries management measures were implemented. In March 2023, the Irish sector of the Whittard Canyon was declared a candidate Special Area of Conservation, particularly for the protection of the Annex I habitat type 'reefs' (NPWS 2023). However, fishing with bottom-contact gear has been banned in EU waters below 800 m water depth since 2017, with a further ban between 400 and 800 m in selected areas brought in to protect vulnerable marine ecosystems in 2022 (EU 2022).

Hydrodynamic mooring

A moored, downward-looking, 600 kHz Acoustic Doppler Current Profiler (ADCP) (M1 mooring in Fig. 1b: 30 m above seafloor and 1500 m water depth) was deployed in the Eastern Branch and recorded near-bed hydrodynamic conditions from June 2019 to June 2020, including vigorous (up to 1 m s^{-1}) internal tides and six turbidity currents. These turbidity currents had maximum down-canyon velocities of 1.5–5.0 m s^{-1}, flow thicknesses greater than 30 m and carried quartz-rich, fine sand as sampled in a sediment trap 10 m above the seafloor (Heijnen *et al.* 2022; Chen *et al.* 2025) (Fig. 3b). The frequency and velocity of the turbidity currents recorded by the ADCP during the sampling period documented how the Whittard Canyon experienced turbidity current activity analogous

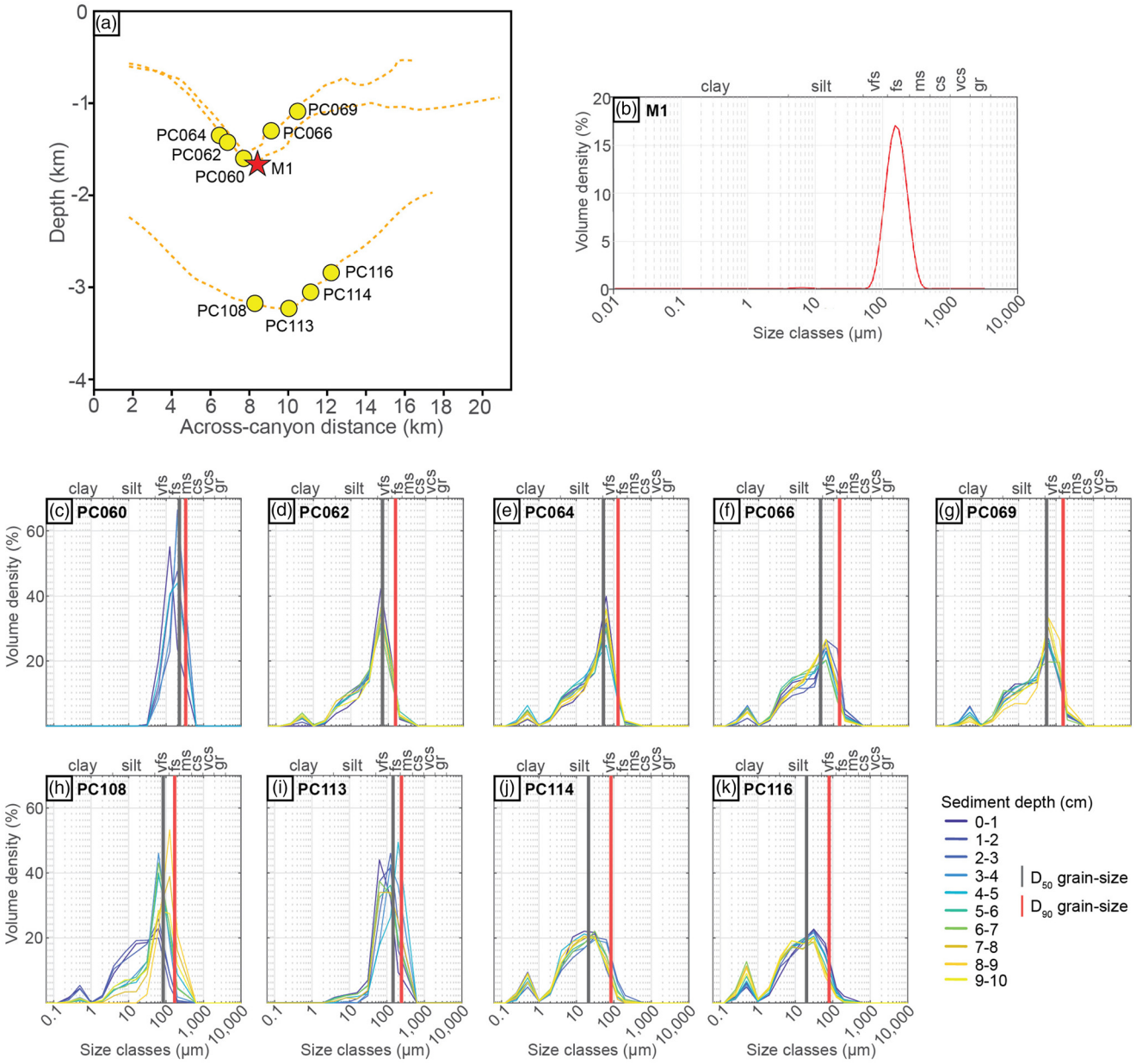

Fig. 3. (**a**) Cross-section of the samples for grain-size analysis. (**b**) Grain-size distribution plots for the sediment trap at the M1 mooring site of Heijnen *et al.* (2022). (**c**)–(**k**) the push cores of the current study. Abbreviations: vfs, very fine sand; fs, fine sand; ms, medium sand; cs, coarse sand; vcs, very coarse sand; gr, granule.

in frequency and velocity to many land-attached canyons, despite being land-detached (Heijnen *et al.* 2022; Talling *et al.* 2023).

Sediment push-core recovery

Five precisely located push cores were collected using the ROV *Isis* during expedition JC237 onboard the RRS *James Cook* (Huvenne 2024), along an across-canyon transect in the upper-canyon reach (24.9 km from the head and 1062–1546 m water depth) from 34 to 521 m above thalweg on the canyon flank. Four precisely located push cores were also collected from an across-canyon transect in the lower-canyon reach (62.3 km from the head and 2773–3204 m water depth) (Fig. 1b, d, e) from 0 to 431 m above thalweg on the canyon flank. In doing so, the two distinct physiographical domains, with respect to the amount of canyon confinement provided by the gradient of the canyon flanks and canyon thalweg of the Whittard Canyon, were extensively sampled. Expanding on the study by Chen *et al.* (2025) where push cores were collected along a down-thalweg transect, the current study used two across-canyon transects. These across-canyon transects were positioned to constrain anthropogenic microparticle distribution and concentration with increasing height and distance from the thalweg, where hydrodynamic processes other than turbidity currents are active. The push cores were recovered from the upper-canyon transect on 21 August 2022, and from the lower-canyon transect on 2 September 2022. All nine push cores were subsampled at 1 cm depth intervals, down to 10 cm, depending on the core recovery (subsample $n = 83$), for anthropogenic microparticle extraction and sediment grain-size analysis (see Supplementary Table S1). High-resolution bathymetric data enabled investigation of the effects of submarine canyon geomorphology on the anthropogenic microparticle distribution.

Laboratory procedures

Anthropogenic microparticle extraction, identification and quantification

The 1 cm sediment core horizons had variable weights and water content, so samples were dried overnight in a drying oven set to

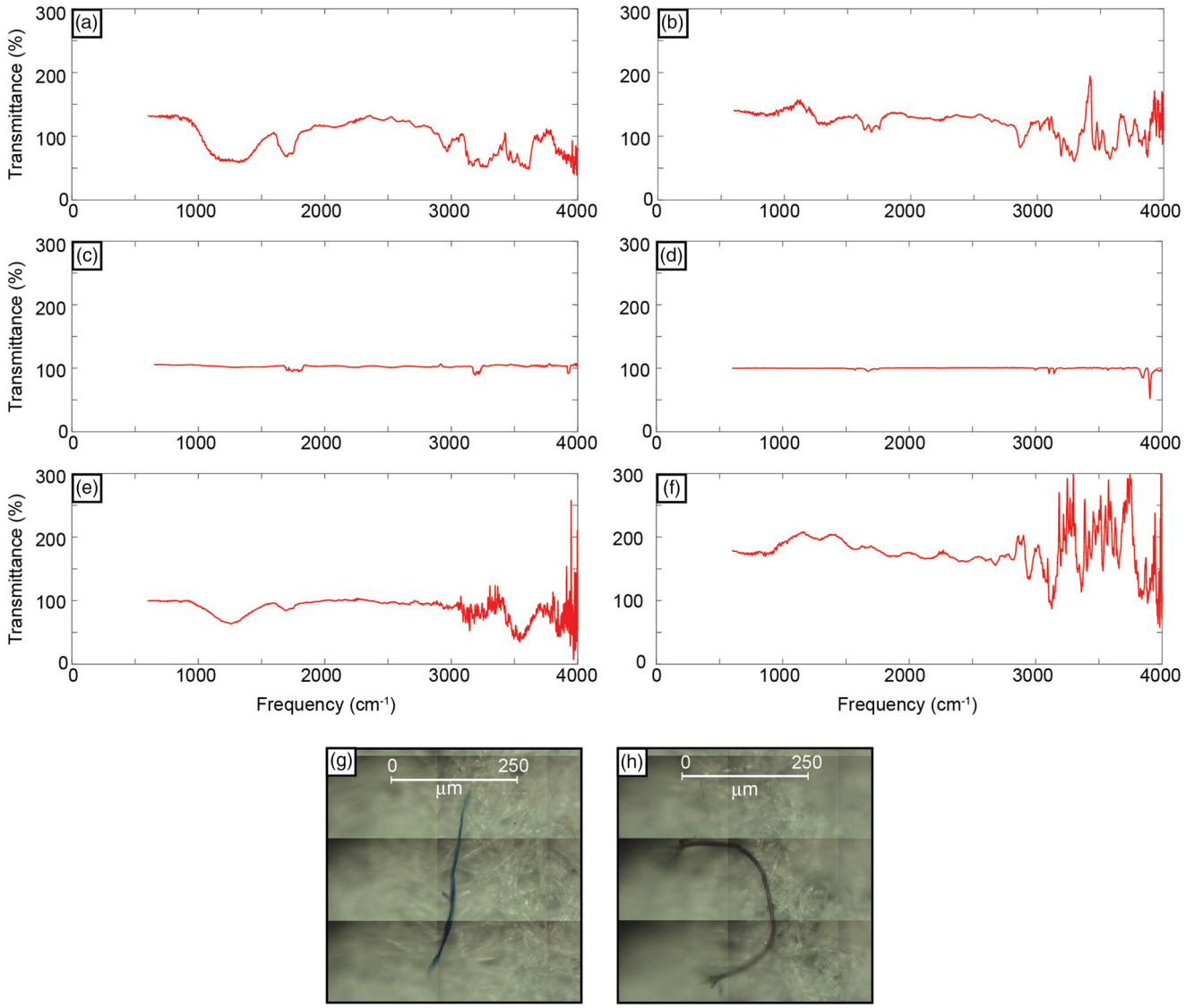

Fig. 4. Micro-Fourier transform infrared (µ-FTIR) spectroscopy spectra and microscope photographs of microfibres. (**a**) Rayon µ-FTIR spectra. (**b**) Polyester µ-FTIR spectra. (**c**) Polyethylene µ-FTIR spectra. (**d**) Polystyrene µ-FTIR spectra. (**e**) Chlorinated rubber µ-FTIR spectra. (**f**) Polypropylene µ-FTIR spectra. (**g**) Photograph of polyester microfibre. (**h**) Photograph of rayon microfibre.

50°C. The dried samples were weighed, and, for comparative purposes, the weight and anthropogenic microparticle content were normalized to 50 g dry sediment weight. Sediment samples were then stored in glass beakers covered with aluminium foil. Samples were added to a 1 l glass beaker with *c*. 700 ml of a dense $ZnCl_2$ solution (1.6 g cm^{-3}), disaggregated using a magnetic stirrer and mixed until homogenized. The microplastics were extracted from the sediment using a polyvinyl chloride Sediment Microplastic Isolation (SMI) unit following a protocol developed for microplastic extraction in a cost-effective, reproducible and easily portable manner (Coppock *et al.* 2017). The solution was added to the SMI unit, and the beaker was rinsed with the $ZnCl_2$ solution to flush any remaining sediment/anthropogenic microparticles. Prior to each use, the SMI unit was disassembled and thoroughly rinsed with Class 1 Milli-Q de-ionized water. Following settling overnight, the headspace supernatant was isolated by closing the ball valve of the SMI unit and rinsing with extra $ZnCl_2$ solution to flush any remaining anthropogenic microparticles before vacuum filtering over a Whatman 541, 22 µm, filter paper. The prepared filter paper was then placed in a labelled Petri dish and covered. Throughout the extraction procedure, all individuals wore white cotton laboratory coats and latex gloves. All the extraction stages were performed in a clean laboratory in a fume cupboard. When the sediment samples were mixing in the 1 l beaker, and settling in the SMI units, they were covered with aluminium foil to limit airborne contamination. When it was not possible during the sample preparation to cover the sediment sample with aluminium foil, an opened Petri dish with a blank Whatman 541, 22 µm, filter paper was placed in the fume cupboard and used as a contamination control procedural blank. When the prepared filter paper was exposed during the identification stage, a second contamination control procedural blank was also collected, again using an opened Petri dish with a blank Whatman 541, 22 µm, filter paper placed in the microscopy laboratory (see Supplementary Table S2).

The prepared filter papers, both from the extraction process and the control blanks, were analysed in a clean microscopy laboratory using a Zeiss Axio Zoom, V16 stereomicroscope at ×20–50 magnification. Here, we define anthropogenic microparticles as being between in 1 µm and 1 mm in size; the same size range used by prominent microplastic studies (e.g. Browne *et al.* 2011; Claessens *et al.* 2011; Van Cauwenberghe *et al.* 2013, 2015; Vianello *et al.* 2013; Dekiff *et al.* 2014; Kane and Clare 2019; Kane *et al.* 2022). Filter papers were traversed systematically to identify anthropogenic microparticles based on the following criteria: (i) no visible cellular or organic structures; (ii) a positive reaction to the hot needle test (de Witte *et al.* 2014); and (iii) maintenance of

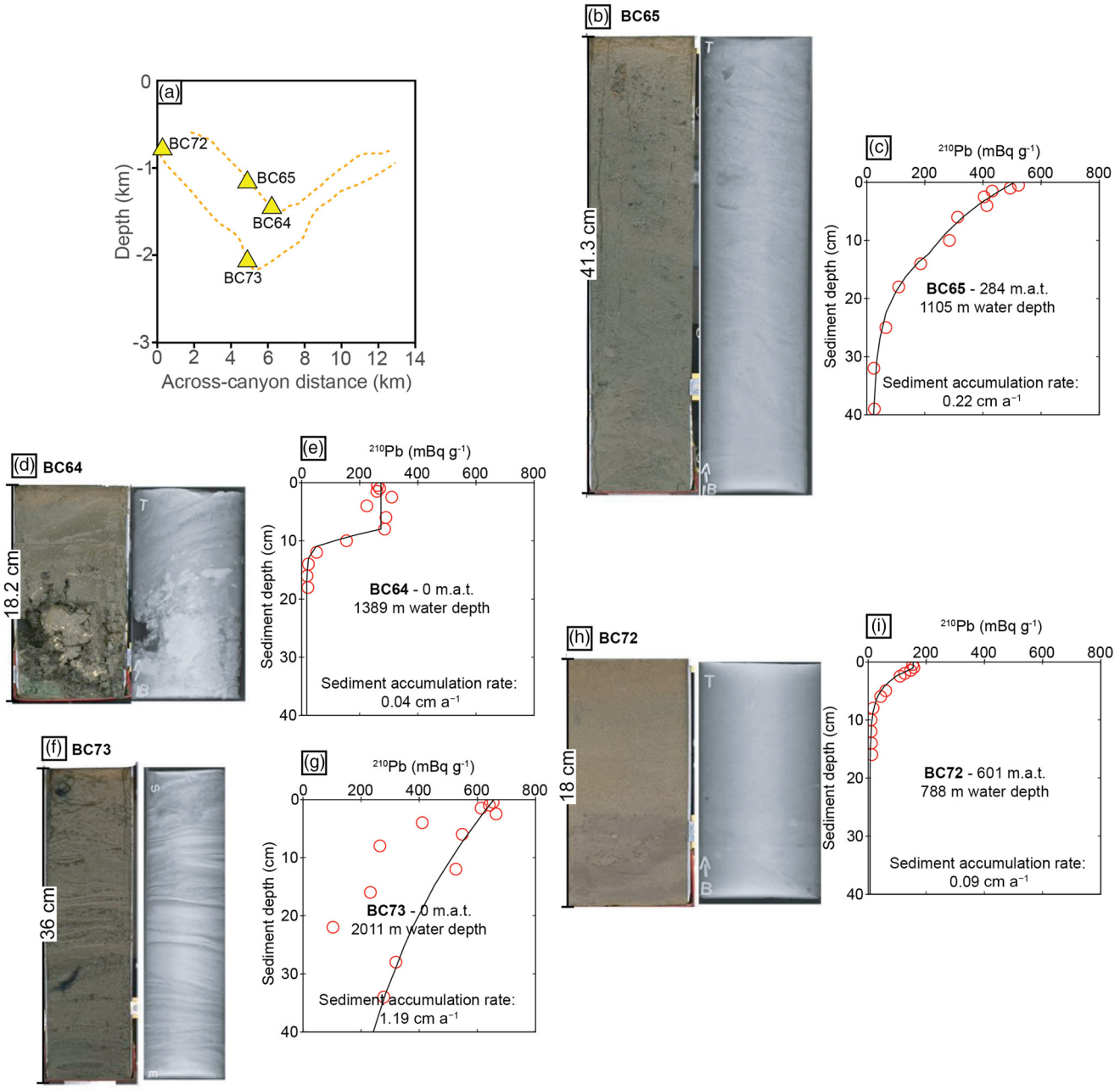

Fig. 5. (**a**) Cross-section showing the locations of the box cores used in the ^{210}Pb dating. (**b**)–(**i**) Core photographs and sediment accumulation rate plots for the box cores: (b) and (c) box core 65; (d) and (e) box core 64; (f) and (g) box core 73; and (h) and (i) box core 72. Abbreviation: m.a.t., metres above thalweg.

structural integrity when touched or moved. Anthropogenic microparticles were categorized based on their colour and type, including, whether they were microfibres, microplastic fragments (including films) or microbeads (see Supplementary Table S1).

Micro-Fourier transform infrared spectroscopy

Anthropogenic microparticles were visually identified using optical microscopy, and a subset of particles was analysed using micro-Fourier transform infrared (μ-FTIR) spectroscopy for polymer confirmation. Identification of the polymer composition was conducted on a subsample ($n = 13$) of the extracted microplastics using a Perkin-Elmer Spotlight 400 FTIR spectrometer in the transmittance mode (Fig. 4; see also Supplementary Table S3). Further details are included in the Supplementary material.

Grain-size analysis

The grain sizes of 79 of the 83 push-core samples were analysed using a Microtrac FLOWSYNC particle sizer (Microtrac MRB). The grain sizes of the four remaining samples (PC060B-E) were analysed using the dry sieving method as the FLOWSYNC particle sizer has an upper particle size limit of 2000 μm, and the fragmented shell material in the samples exceeded this upper limit. The FLOWSYNC particle sizer uses tri-laser diffraction to measure the particle-size distribution with a lower particle limit size of 0.01 μm. The samples were subjected to a small amount of ultrasonic dispersion. Three aliquots were analysed to ensure that each sample was completely dispersed. The grain-size distribution, indicating the volume percentage of grains in a certain size interval, was constructed (Fig. 3c–k). The grain-size percentiles were exported from the FLOWSYNC software and are documented in Supplementary Table S1.

^{210}Pb sediment accumulation rates

Sediment accumulation rates derived from the ^{210}Pb dating of box cores were determined at four positions within the upper-canyon reach: two in the thalweg and two on the canyon flanks (Figs 1 and 5; see Supplementary Table S4). Sediment accumulation rates were calculated from the four box cores (BC64, BC65, BC72 and BC73) (Fig. 5b–i; see Supplementary Table S4) using ^{210}Pb dating. The box cores were collected during the research cruise 64PE421 conducted by NIOZ (the Royal Netherlands Institute for Sea Research) from 14 to 25 May 2017. The recovery rates of the box cores varied by location. Further details are included in the Supplementary material.

Results

Anthropogenic microparticle pollution in surficial sediments

Anthropogenic microparticles were present throughout all nine push cores (Figs 6 and 7c, f). A total of 1255 anthropogenic microparticles were observed with optical microscopy and a subset of the particles ($n = 13$) was verified with FTIR spectroscopy. Microfibres were the dominant anthropogenic microparticle type (microfibres = 91.3%, fragments = 5.7% and microbeads = 3.0%). Herein, the anthropogenic microparticle count quantifies as the number of particles per 50 g of dry sediment weight (particles/50 g). The FTIR spectroscopy confirmed that 62% of the anthropogenic microparticles were plastic, with common polymers including polyvinyl butyral, polyvinylchloride and acrylic. The remaining 38% comprised semi-synthetic polymers, including chlorinated rubber and rayon (Fig. 4; see Supplementary Table S3).

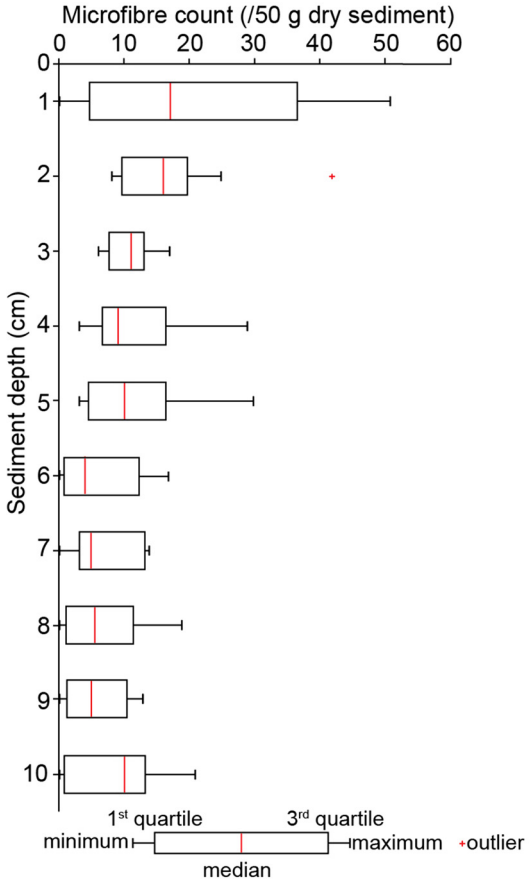

Fig. 6. Box plot for the microfibre concentration and sediment depth for all the push cores.

Microfibres in the canyon thalweg

In push core 060 (PC060) (34 m above thalweg, at the upper transect), the grain-size range was 31–8000 µm, and the gravel and sand percentages had arithmetic means of 9.6 and 90.3%, respectively; the granule-sized particles were fragmented shells (Fig. 3c; see Supplementary Table S1). The microfibre count in PC060 increased with sediment depth from 4 to 30 microfibres/50 g (Fig. 7c). In PC113 (0 m above thalweg, at the lower transect), the grain-size range was 2–200 µm, and the sand and silt percentages had arithmetic means of 92.4 and 7.6%, respectively (Fig. 3i; see Supplementary Table S1). The microfibre count in PC113 decreased with sediment depth by 62.5% (Fig. 7f).

The sediment accumulation rates in BC64 (1389 m water depth, 0 m above thalweg) and BC73 (2011 m water depth, 0 m above thalweg) were 0.04 and 1.19 cm a^{-1}, respectively (Fig. 5e, g). Therefore, it could take 8.4–250 years to accumulate 10 cm of sediment in the canyon thalweg, meaning that sediments containing anthropogenic microparticles in the thalweg may predate the mass production of plastic in the 1950s. The mobility of sediment within the thalweg can be observed in a photograph captured by the ROV *Isis* during the recovery of PC060; a high level of suspended sediment is recorded in the water column of the thalweg following the passing of a turbidity current down-canyon (Fig. 8a).

Microfibres on the canyon flanks

At the upper transect, the push cores (PC062, PC064 and PC066, located 220, 277 and 321 m above thalweg, respectively) had a grain-size range of 0.25–200 µm (clay to fine sand) (Fig. 3d–f), and the sand percentage had arithmetic means of 54.9, 43.8 and 39.9%, respectively (see Supplementary Table S1). The microfibre count in these cores was low and uniform, ranging from 0 to 19/50 g with an arithmetic mean of 7/50 g (Fig. 7c). PC069 (518 m above thalweg) was located near the tributary canyons at the upper transect; the grain-size range was also 0.25–200 µm, yet, despite its increased height above the central thalweg, the sand percentage had an arithmetic mean of 47.6% (Fig. 3f, g; see Supplementary Table S1). PC069 contained the greatest range of anthropogenic microparticle types, and an arithmetic mean microfibre count of 18/50 g (Fig. 7c; see Supplementary Table S1). At the lower transect, PC114 and PC116, located 209 and 431 m above thalweg, respectively, had the same grain-size range as the canyon-flank push cores at the upper transect, but the sand percentage had arithmetic means of 17.2 and 16.5%, respectively (Fig. 3j, k; see Supplementary Table S1). In these push cores, the microfibre count decreased with depth by 64.5 and 80.3%, respectively (Fig. 7f; see Supplementary Table S1).

The sediment accumulation rates in BC65 (1105 m water depth and 284 m above thalweg) and BC72 (788 m water depth and 601 m above thalweg) were 0.22 and 0.09 cm a^{-1}, respectively (Fig. 5c, i). Therefore, it could take 45–111 years to accumulate 10 cm of sediment on the canyon flanks and this means that sediment containing anthropogenic microparticles on the canyon flanks may predate the mass production of plastic.

On the canyon flanks at the upper transect, 277 m above thalweg and thus above the known thickness of the turbidity currents recorded by Heijnen *et al.* (2022), the crest orientation of sub-parallel ripples observed on the seafloor suggests a flow direction approximately perpendicular to the direction of turbidity current transport (Fig. 8b). This indicates that other hydrodynamic processes capable of sediment transport are also active on the canyon flanks (e.g. internal tides).

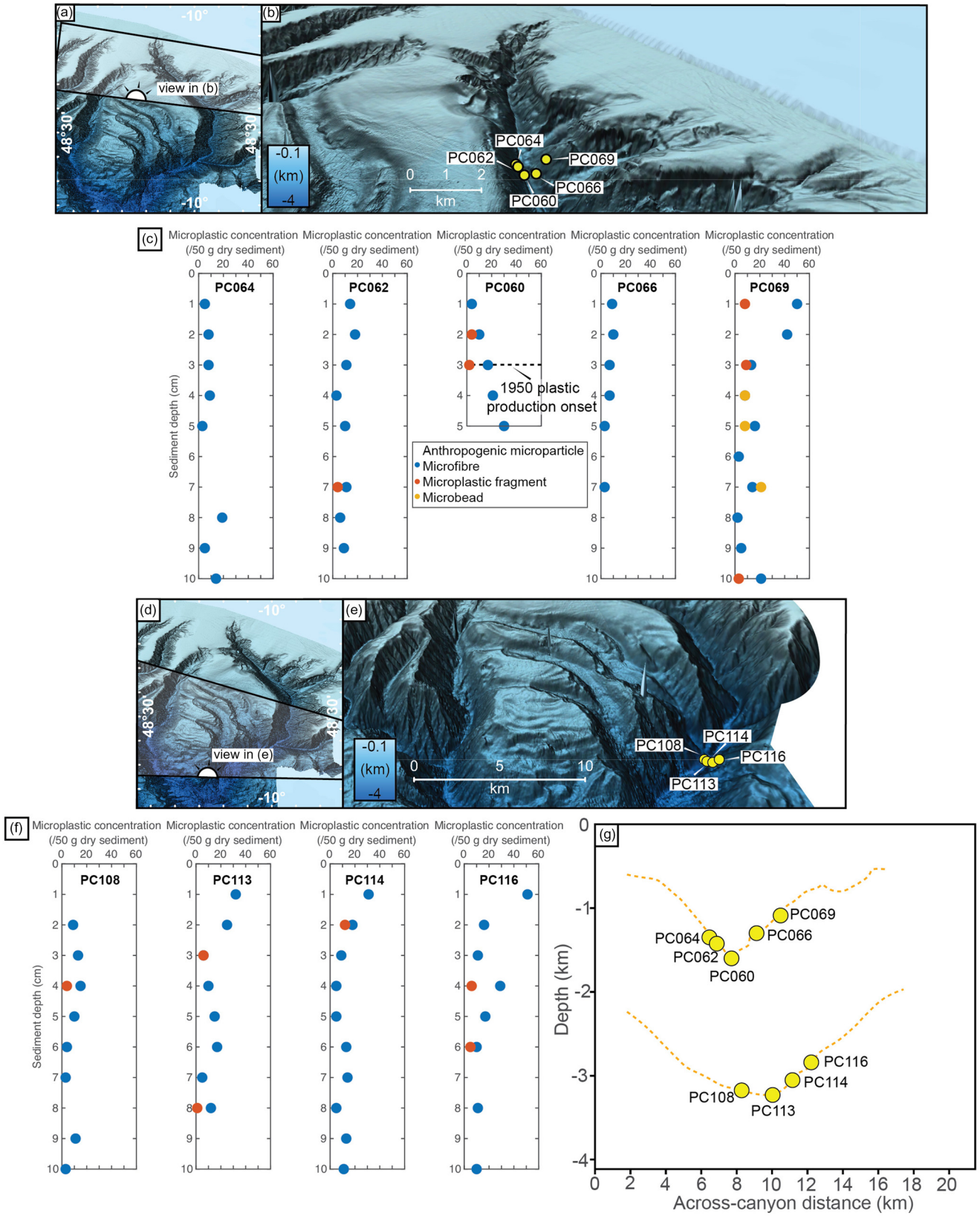

Fig. 7. Anthropogenic microparticle count with sediment depth for the push cores located in the Whittard Canyon. (**a**), (**b**), (**d**) and (**e**) Location maps and high-resolution bathymetric maps of the Eastern Branch. ×3 vertical exaggeration. (**c**) and (**f**) Anthropogenic microparticle trends for each push core. (**g**) Cross-section of the Whittard Canyon showing the push-core locations. In PC060, the 1950 plastic production onset is based on the sediment accumulation rate calculated from ^{210}Pb dating of the sediments in box core 64. The sediment accumulation rate calculated from BC65 can be approximately tied to PC064 and equates to 16.5 cm of sediment accumulation in the 75 year period since the onset of plastic production. The push cores and box cores are not co-located within the Whittard Canyon but are based on their longitudinal position and height above the thalweg; they are deemed suitable for relating sediment accumulation rate to the presence of anthropogenic microparticles with depth.

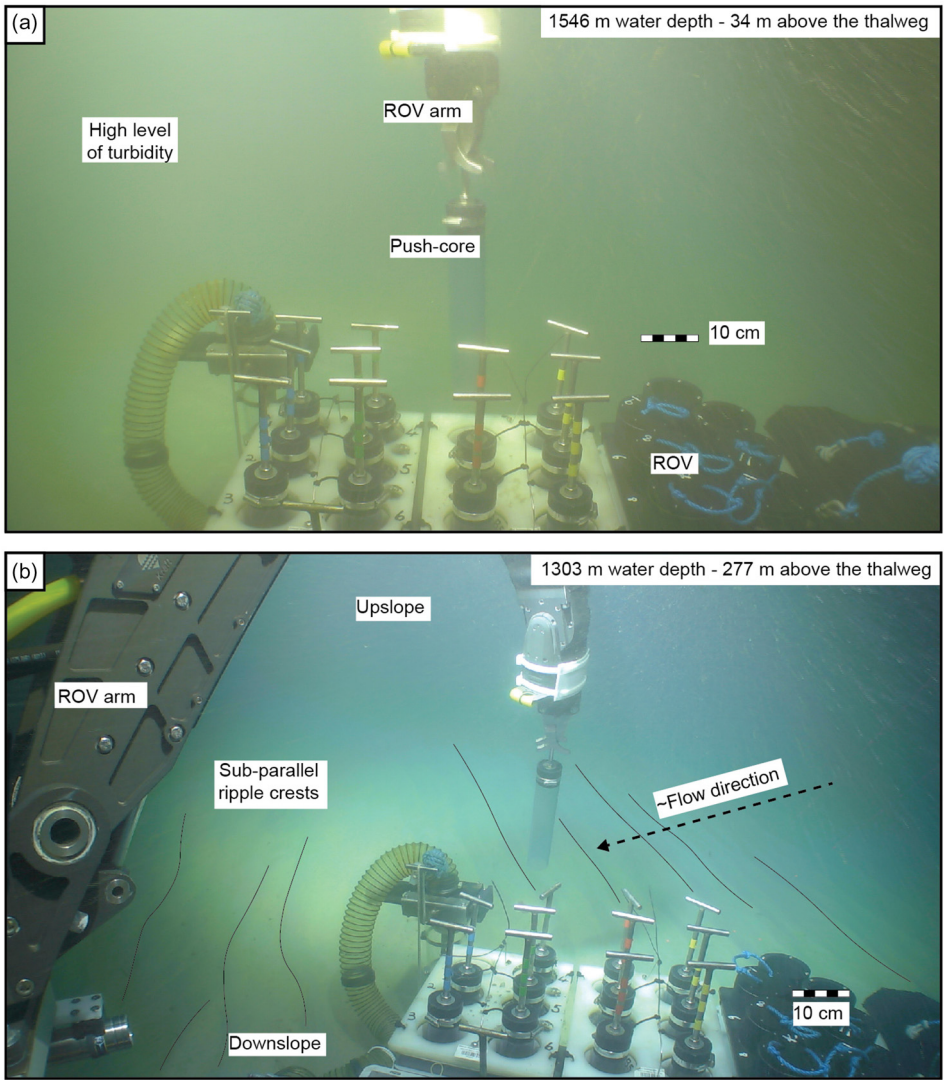

Fig. 8. Photographs taken of seabed push-core sampling from the ROV. (**a**) Canyon thalweg at the upper transect. (**b**) Canyon flanks at the upper transect.

Discussion

Microfibre transport and burial processes

Microfibre pollution is pervasive throughout the Eastern Branch down to the 10 cm sediment depth of the push cores. Almost all push cores showed a gradual decline in microfibre concentration with depth. This gradual decline with depth is despite the marked differences in sediment accumulation rates across the canyon, and the 700% increase in the background plastic production rate. Microfibres are hypothesized to be transported to the canyon head via cross-continental shelf currents, and transported through the canyon by turbidity currents (Fig. 9a, c) (Chen *et al.* 2025) and via vertical settling from marine sources (Fig. 9b, f), but their subsequent redistribution and burial cannot solely be explained by deposition from turbidity currents.

From the observed grain-size trends in the canyon thalweg (notably the absence of sediment <31 μm in PC060) we infer that the frequent (sub-annual) and fast (up to 5 m s^{-1}) turbidity currents serve to bypass and winnow silt-sized sediment and microfibres further down-canyon. Pohl *et al.* (2020) explored how the vertical distribution of microfibres was more homogeneous in turbidity currents compared to microplastic fragments. Furthermore, Chen *et al.* (2025) suggest that the flushing of microfibres and other types of anthropogenic microparticles by turbidity currents in the Whittard Canyon occurs due to their markedly lower settling velocity compared to quartz grains (see fig. 4 in Chen *et al.* 2025). This suggests that anthropogenic microparticles are capable of being transported in the dilute, upper parts of turbidity currents, through submarine canyons and farther into the deep sea to a wider range of depositional environments and seafloor ecosystems.

However, microfibres were recorded at elevations up to 518 m above thalweg, over an order of magnitude above the recorded thickness of measured turbidity currents. This suggests that other processes are also important in the Whittard Canyon and need be considered in other submarine canyon systems in order to develop holistic source-to-sink models for anthropogenic pollutant transfer (Fig. 9). The presence of sand in the canyon-flank push cores, and increased sand percentage 518 m above thalweg, suggests that sediment is not sourced exclusively from hemipelagic fallout. Furthermore, this suggests that sediment, and microfibres and other anthropogenic microparticles, stored on the Celtic Margin are being transported via episodic turbidity currents in the tributary canyons or by sediment resuspension by benthic trawling close to the canyon head and on the canyon interfluves (Figs 2, 3g and 9; see Supplementary Table S1). The location of BC72 (Fig. 5a), high on the canyon flank opposite the Celtic Margin and the tributary canyons, could explain the low sediment accumulation rates (Fig. 5i).

The observed uniformity of the gradual decline in microfibre concentration with sediment depth suggests, however, that sub-seafloor processes also affect microfibre burial processes in the deep sea. Hyporheic transfer of microplastics has been demonstrated in riverbeds (Frei *et al.* 2019). In sub-seafloor settings, hyporheic

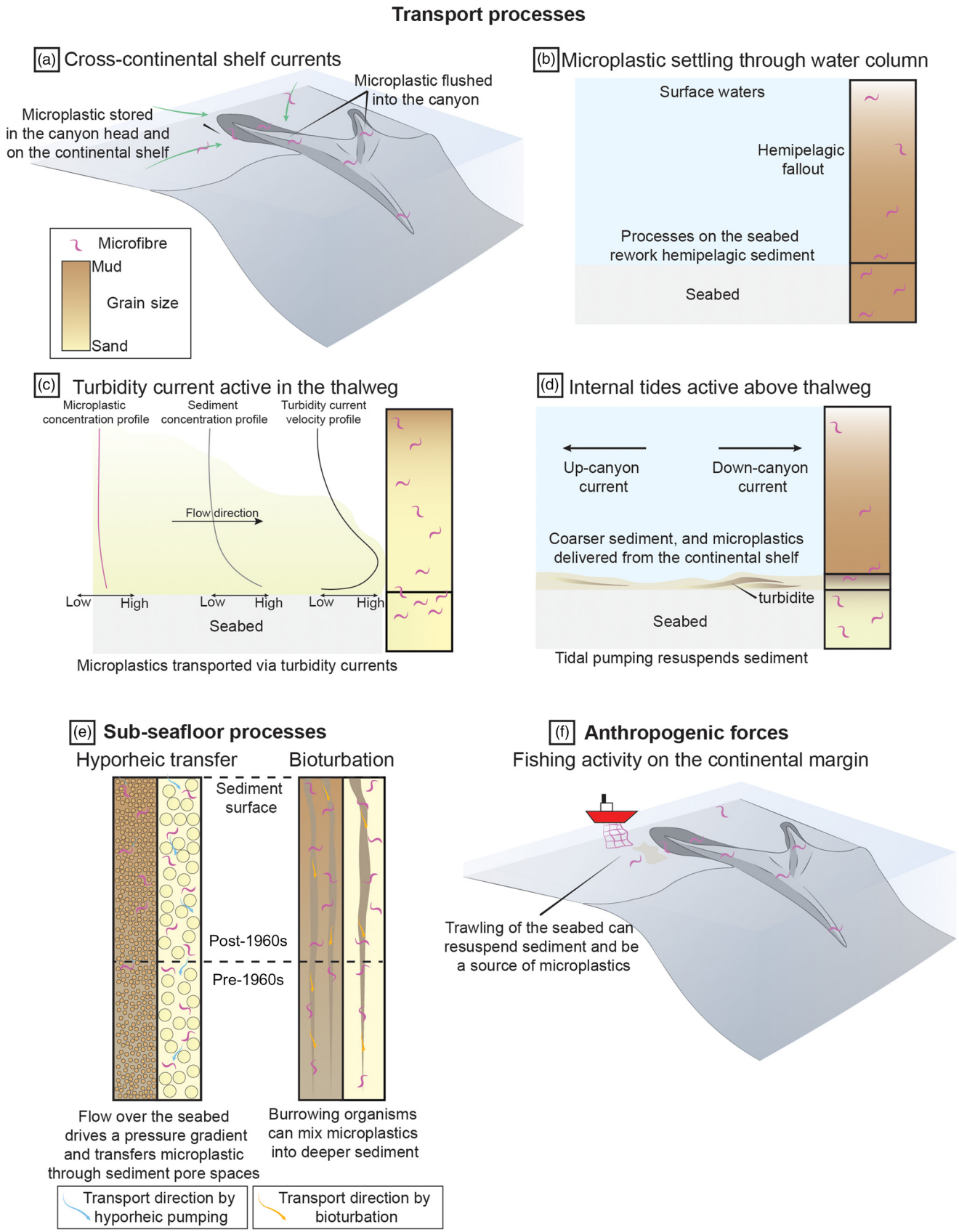

Fig. 9. Synthesis of microfibre transport and burial processes in submarine canyons. (**a**)–(**d**) Transport processes. (**e**) Sub-seafloor processes. (**f**) Anthropogenic forces.Source: (c) is modified from Chen *et al.* (2025).

transfer is driven by pressure gradients, as exist between the base of turbidity currents and the seafloor (e.g. Eggenhuisen and McCaffrey 2012), and is invoked here as a control on the stratigraphic distribution of microfibres (Fig. 9e). Internal tides have been directly monitored in the Whittard Canyon (Hall *et al.* 2017) and have been observed to reflect against the steep topography of the canyon flanks in the upper canyon where they are then focused into the canyon thalweg (Amaro *et al.* 2016; Hall *et al.* 2017; van Haren

et al. 2022). This is hypothesized to cause sediment and microfibre resuspension via internal tide pumping (Fig. 9d) (e.g. Li *et al.* 2019; Normandeau *et al.* 2024). In other submarine canyons, internal tides have been observed to rework turbidity current deposits (Normandeau *et al.* 2024), and affect particulate organic carbon transport (Maier *et al.* 2019). Particulate organic carbon shares similar hydrodynamic properties to anthropogenic microparticles in terms of density and irregular dimensions. On the canyon flanks of the Whittard Canyon internal tide pumping may generate a sufficient pressure gradient to drive hyporheic transfer of microfibres through sediment pore spaces, where turbidity currents are not active. Microplastic infiltration depth increases positively with sediment grain size (Waldschläger and Schüttrumpf 2020); hence, hyporheic transfer may be enhanced in the canyon thalweg where turbidity currents and internal tide focusing are active, compared to high on the canyon flanks where turbidity currents are absent (Fig. 9e).

Bioturbation may also play a role in controlling the vertical distribution of microfibres in the sub-seafloor (Fig. 9e). The uppermost 10 cm of BC64 and BC65 were bioturbated (Fig. 5b, d). Sediment and microplastic mixing by bioturbation has been documented experimentally (Näkki *et al.* 2017) and is hypothesized to occur in deep-sea sediments (Courtene-Jones *et al.* 2020). The depth of the bioturbated layer extends to 10 cm in modern marine sediments, with individual burrows extending deeper (Tarhan *et al.* 2015). This mixing may be enhanced on the canyon flanks due to less stressed conditions for organisms to colonize compared to the thalweg (Fig. 9e). However, a diverse suite of burrow types has been recorded in the margin of slope channel fills where organisms can 'shelter' from powerful sediment gravity flows (Heard and Pickering 2008; Hubbard *et al.* 2012). This has the potential to further complicate sediment and microplastic mixing mechanisms in surficial submarine canyon sediments. Bioturbation and hyporheic transfer are likely to be important in transferring anthropogenic microparticles into pre-1950s deep-sea sediments; the latter supported in lakes where bioturbation is absent (Dimante-Deimantovica *et al.* 2024). The identification of a sharp, laterally continuous contact between sediments of pre-plastic production age, with an absence of anthropogenic microparticles, and of post-plastic production age, containing anthropogenic microparticles, is required to support the formal definition of the Anthropocene. In reality, this will be challenging due to the interaction of post-depositional processes in terrestrial and deep-marine sediments.

Shredding of anthropogenic microparticle signals in the deep-sea

We suggest that sediment transport and burial processes, and anthropogenic forcing, act as non-linear filters that can shred the environmental signal of increasing plastic production rates through time in submarine canyons. The efficiency of anthropogenic microparticle transfer from land-based sources to the Whittard Canyon is relatively low, given the land-detached nature of the canyon. This suggests that anthropogenic microparticle pollution in land-detached canyons, of which there are more than 5000 (Harris and Whiteway 2011), may be dominantly marine-sourced, and that such systems receive a buffered supply of terrestrially sourced anthropogenic microparticles. Despite this, Chen *et al.* (2025) showed that the maximum microplastic concentration per 50 g of dry sediment in the Whittard Canyon was greater than that recorded in other submarine canyons. Combined with the study of Chen *et al.* (2025), the anthropogenic microparticle distribution (Fig. 7c, f) and grain-size data (Fig. 3c–k) presented here suggest that anthropogenic microparticles are capable of being transported through the Whittard Canyon and are hypothesized to be transferred down-canyon to the Celtic Fan at water depths of more than 4500 m. Given the importance of the deep sea being the ultimate sink to anthropogenic microparticles (Kane and Clare 2019), how they are distributed in submarine fan successions and their relationship with respect to sediment depth and age should be the focus of future attempts to further understand micropollutant distribution in the deep sea. Furthermore, given the dynamism of submarine canyons, the buffered supply of anthropogenic microparticles to land-detached canyons, and the mobility of microfibres and thus other anthropogenic microparticles in the sub-seafloor, the efficacy of using anthropogenic microparticles as anthropogenic tracer particles is questionable, along with calculations of their fluxes.

Conclusions

By adopting a multi-disciplinary approach, our results show that anthropogenic microparticle pollution is pervasive in the Whittard Canyon, at least to 10 cm sediment depth in both the thalweg and on canyon flanks more than 500 m above the thalweg. While turbidity currents are a major agent in the transfer of anthropogenic microparticles, the turbidity currents in the Whittard Canyon are only tens of metres thick, suggesting other processes and sources of anthropogenic microparticles are needed to explain their distribution. These processes are under-represented in the stratigraphic record of deep-sea deposits, and a better understanding can aid more accurate calculations of particulate matter flux. Additional sources include hemipelagic settling, and sediments on the continental shelf resuspended by benthic trawling and entering tributary canyons. Transport and resuspension of anthropogenic microparticles by internal tidal pumping is likely to occur across the entire canyon water depth. Almost all of the push cores showed only a gradual decline in anthropogenic microparticle concentrations down to 10 cm, despite the 700% increase in global plastic production since the 1970s. Where low sedimentation accumulation rates are recorded, much of the sediment in the box cores predates plastic production. This suggests subsurface mobility of anthropogenic microparticles, with the likely processes including bioturbation and hyporheic transfer. The observed distribution of anthropogenic microparticles in the Whittard Canyon demonstrates that they are not entirely flushed through canyons, but may be permanently or transiently stored, and be mobile within the sediment bed. These results suggest that anthropogenic microparticles incorporated into deep-sea sediments may be a poor record of canyon particulate flux and form an imperfect timeline, meaning that identifying the Anthropocene boundary using anthropogenic microparticles in these sediments may be flawed. A multi-disciplinary approach is critical to untangling the different processes that act to transfer and bury micropollutants in deep-sea sediments, and to identify seafloor ecosystems that are vulnerable to anthropogenic micropollutant exposure.

Scientific editing by Gene Rankey

Acknowledgements We thank the captain, crew and technical teams of the RSS *James Cook* cruise JC237, particularly the ROV *Isis* team for the sample acquisition.. We would like to thank Dr H. de Stigter for help with the ^{210}Pb measurements. H. Brown of the University of Leeds, and T. Bishop and J. Yarwood of the University of Manchester are thanked for help with analyses. Subject editor Gene Rankey and reviewers Zane Jobe and Jon Rotzien are gratefully acknowledged for their constructive comments that helped to improve the manuscript.

Author contributions **EK**: conceptualization (lead), formal analysis (lead), investigation (lead), methodology (equal), visualization (lead), writing – original draft (lead); **IAK**: conceptualization (supporting), funding acquisition (supporting), methodology (supporting), project administration (equal), resources (lead), supervision (equal), writing – review & editing (equal); **MAC**: conceptualization (supporting), funding acquisition (equal), project

administration (supporting), resources (equal), writing – review & editing (supporting); **DMH**: conceptualization (supporting), project administration (supporting), supervision (lead), writing – review & editing (supporting); **VAIH**: investigation (supporting), project administration (supporting), writing – review & editing (supporting); funding acquisition (equal); **EJS**: investigation (supporting), writing – review & editing (supporting); **JP**: conceptualization (supporting), supervision (supporting), writing – review & editing (supporting); **FM**: funding acquisition (supporting), investigation (supporting), project administration (supporting); **JK**: formal analysis (supporting), methodology (supporting), visualization (supporting).

Funding The RSS *James Cook* cruise JC237 was supported by the UK National Environmental Research Council (NERC) National Capability Programme (grant No. NE/R015953/1; recipients M.A. Clare and V.A.I. Huvenne) 'Climate Linked Atlantic Sector Science'. M.A. Clare and V.A.I. Huvenne also acknowledge funding from the NERC National Capability Programme: Atlantic Climate and Environment Strategic Science and MISSING LINK (grant No. NE/Y005589/1). F. Mienis and J. Kranenburg were supported by the Innovational Research Incentives Scheme of the Netherlands Organization for Scientific Research (NWO-VIDI grant No. 0.16.161.360).

Competing interests The authors declare that they have no known competing financial interests or personal relationships that could have appeared to influence the work reported in this paper.

Data availability All data generated or analysed during this study are included in this published article (and if present, its supplementary information files).

References

Amaro, T., Huvenne, V.A.I. *et al.* 2016. The Whittard Canyon – a case study of submarine canyon processes. *Progress in Oceanography*, **146**, 38–57, https://doi.org/10.1016/j.pocean.2016.06.003

Andrady, A.L. 2011. Microplastics in the marine environment. *Marine Pollution Bulletin*, **62**, 1596–1605, https://doi.org/10.1016/j.marpolbul.2011.05.030

Athey, S.N. and Erdle, L.M. 2022. Are we underestimating Anthropogenic microfibre pollution? A critical review of occurrence, methods, and reporting. *Environmental Toxicology and Chemistry*, **41**, 822–837, https://doi.org/10.1002/etc.5173

Bailey, L.P., Clare, M.A. *et al.* 2024. Highly variable deep-sea currents over tidal and seasonal timescales. *Nature Geoscience*, **17**, 787–794, https://doi.org/10.1038/s41561-024-01494-2

Belzagui, F., Buscio, V., Gutiérrez-Bouzán, C. and Vilaseca, M. 2021. Cigarette butts as a microfibre source with microplastic level of concern. *Science of the Total Environment*, **762**, https://doi.org/10.1016/j.scitotenv.2020.144165

Brandon, J.A., Jones, W. and Ohman, M.D. 2019. Multidecadal increase in plastic particles on coastal ocean sediments. *Science Advances*, **5**, https://doi.org/10.1126/sciadv.aax0587

Browne, M.A., Crump, P., Niven, S.J., Teuten, E., Tonkin, A. and Galloway, T. 2011. Accumulation of microplastic on shorelines worldwide: sources and sinks. *Environmental Science & Technology*, **45**, 9175–9179, https://doi.org/10.1021/es201811s

Chen, M., Du, M. *et al.* 2020. Forty-year pollution history of microplastics in the largest marginal sea of the western Pacific. *Geochemical Perspective Letters*, **13**, 42–47, https://doi.org/10.7185/geochemlet.2012

Chen, P., Kane, I.A., Clare, M.A., Soutter, E.L., Mienis, F., Wogelius, R.A. and Keavney, E. 2025. Direct evidence that microplastics are transported to the deep sea by turbidity currents. *Environmental Science & Technology*, **59**, 7278–7287, https://doi.org/10.1021/acs.est.4c12007

Choy, C.A., Robison, B.H. *et al.* 2019. The vertical distribution and biological transport of marine microplastics across the epipelagic and mesopelagic water column. *Scientific Reports*, **9**, 7843, https://doi.org/10.1038/s41598-019-44117-2

Claessens, M., De Meester, S., Van Lunduyt, L., De Clerck, K. and Janssen, C.R. 2011. Occurrence and distribution of microplastics in marine sediments along the Belgian coast. *Marine Pollution Bulletin*, **62**, 2199–2204, https://doi.org/10.1016/j.marpolbul.2011.06.030

Coppock, R.L., Cole, M., Lindeque, P.K., Queirós, A.M. and Galloway, T.S. 2017. A small-scale portable method for extracting microplastics from marine sediments. *Environmental Pollution*, **230**, 829–837, https://doi.org/10.1016/j.envpol.2017.07.017

Courtene-Jones, W., Quinn, B., Ewins, C., Gary, S.F. and Narayanaswamy, B.E. 2020. Microplastic accumulation in deep-sea sediments from the Rockall Trough. *Marine Pollution Bulletin*, **154**, https://doi.org/10.1016/j.marpolbul.2020.111092

Curray, J. and Moore, D.G. 1971. Growth of the Bengal Deep-Sea Fan and denudation in the Himalayas. *Geological Society of America Bulletin*, **87**, 563–572, https://doi.org/10.1130/0016-7606(1971)82[563:GOTBDF]2.0.CO;2

Daly, E., Johnson, M.P., Wilson, A.M., Gerritsen, H.D., Kirakoulakis, K., Allcock, A.L. and White, M. 2018. Bottom trawling at Whittard Canyon: Evidence for seabed modification, trawl plumes and food source heterogeneity. *Progress in Oceanography*, **169**, 227–240, https://doi.org/10.1016/j.pocean.2017.12.010

Davies, J.S., Howell, K.L., Stewart, H.A., Guinan, J. and Golding, N. 2014. Defining biological assemblages (biotopes) of conservation interest in the submarine canyons of the South West Approaches (offshore United Kingdom) for use in marine habitat mapping. *Deep-Sea Research Part II: Topical Studies in Oceanography*, **104**, 208–229, https://doi.org/10.1016/j.dsr2.2014.02.001

Dekiff, J.H., Klasmeier, J. and Fries, E. 2014. Occurence and spatial distribution of microplastics in sediments from Norderney. *Environmental Pollution*, **186**, 248–256, https://doi.org/10.1016/j.envpol.2013.11.019

de Witte, B., Devriese, L., Bekaert, K., Hoffman, S., Vandermeersch, G., Cooreman, K. and Robbens, J. 2014. Quality assessment of the blue mussel (*Mytilus edulis*): Comparison between commercial and wild types. *Marine Pollution Bulletin*, **85**, 145–155, https://doi.org/10.1016/j.marpolbul.2014.06.006

Dimante-Deimantovica, I., Saarni, S. *et al.* 2024. Downward migrating microplastics in lake sediments are a tricky indicator for the onset of the Anthropocene. *Science Advances*, **10**, https://doi.org/10.1126/sciadv.adi8136

Eggenhuisen, J.T. and McCaffrey, W.D. 2012. Dynamic deviation of fluid pressure from hydrostatic pressure in turbidity currents. *Geology*, **40**, 295–298, https://doi.org/10.1130/G32627.1

EU 2022. Commission Implementing Regulation (EU) 2022/1614 of 15 September 2022 determining the existing deep-sea fishing areas and establishing a list of areas where vulnerable marine ecosystems are known to occur or are likely to occur. *Official Journal of the European Union*, **242**, 19.9.2022, 1–141, https://data.europa.eu/eli/reg_impl/2022/1614/oj

Fernandez-Arcaya, U., Ramirez-Llodra, E. *et al.* 2017. Ecological role of submarine canyons and need for canyon conservation: a review. *Frontiers in Marine Science*, **4**, https://doi.org/10.3389/fmars.2017.00005

Finnegan, M.D., Süsserott, R., Gabbott, S.E. and Gouramanis, C. 2022. Man-made natural and regenerated cellulosic fibres greatly outnumber microplastic fibres in the atmosphere. *Environmental Pollution*, **310**, https://doi.org/10.1016/j.envpol.2022.119808

Frei, S., Piehl, S., Gilfedder, B.S., Löder, M.G.L., Krutzke, J., Wilhelm, L. and Laforsch, C. 2019. Occurrence of microplastics in the hyporheic zone of rivers. *Scientific Reports*, **9**, e15256, https://doi.org/10.1038/s41598-019-51741-5

Global Fishing Watch 2024. Map & data. Global Fishing Watch, https://globalfishingwatch.org/map/index?start=2024-05-30T00%3A00%3A00.000Z&end=2024-08-30T00%3A00%3A00.000Z&longitude=26&latitude=19&zoom=1.49 [last accessed 25 April 2024].

Hage, S., Baker, M.L. *et al.* 2024. How is particulate organic carbon transported through the river-fed submarine Congo Canyon to the deep sea? *Biogeosciences*, **21**, 4251–4272, https://doi.org/10.5194/bg-21-4251-2024

Hall, R.A., Aslam, T. and Huvenne, V.A. 2017. Partly standing internal tides in a dendritic submarine canyon observed by an ocean glider. *Deep Sea Research Part I: Oceanographic Research Papers*, **126**, 73–84, https://doi.org/10.1016/j.dsr.2017.05.015

Harris, P.T. and Whiteway, T. 2011. Global distribution of large submarine canyons: geomorphic differences between active and passive continental margins. *Marine Geology*, **285**, 69–86, https://doi.org/10.1016/j.margeo.2011.05.008

Heard, T.G. and Pickering, K.T. 2008. Trace fossils as diagnostic indicators of deep-marine environments, Middle Eocene Ainsa-Jaca basin, Spanish Pyrenees. *Sedimentology*, **55**, 809–844, https://doi.org/10.1111/j.1365-3091.2007.00922.x

Heijnen, M.S., Mienis, F. *et al.* 2022. Challenging the highstand-dormant paradigm for land-detached submarine canyons. *Nature Communications*, **13**, e3448, https://doi.org/10.1038/s41467-022-31114-9

Hubbard, S.M., MacEachern, J.A. and Bann, K.L. 2012. Slopes. *In*: Knaust, D. and Bromley, R.G. (eds) *Trace Fossils as Indicators of Sedimentary Environments*. Developments in Sedimentology, **64**. Elsevier, Amsterdam, 607–642.

Huvenne, V.A.I. 2024. *RRS James Cook Expedition 237, 6 August–4 September 2022. CLASS – Climate Linked Atlantic Sector Science: Whittard Canyon and Porcupine Abyssal Plain Fixed Point Observatories*. National Oceanography Centre Research Expedition Report 80. National Oceanography Centre, Southampton, UK, https://www.bodc.ac.uk/resources/inventories/cruise_inventory/reports/jc237.pdf

Jiang, N., Chang, X. *et al.* 2024. Physiological response of mussel to rayon microfibres and PCB's exposure: overlooked semi-synthetic micropollutant. *Journal of Hazardous Materials*, **470**, https://doi.org/10.1016/j.jhazmat.2024.134107

Kane, I.A. and Clare, M.A. 2019. Dispersion, accumulation, and the ultimate fate of microplastics in deep-marine environments: a review and future direction. *Frontiers of Earth Science*, **7**, https://doi.org/10.3389/feart.2019.00080

Kane, I.A., Clare, M.A., Miramontes, E., Wogelius, R., Rothwell, J.R., Garreau, P. and Pohl, F. 2020. Seafloor microplastic hotspots controlled by deep-sea circulation. *Science*, **368**, 1140–1145, https://doi.org/10.1126/science.aba5899

Kane, I.A., Michael, A.C., Miramontes, E., Wogelius, R., Rothwell, J.J., Garreau, P. and Pohl, F. 2022. Seafloor microplastic hotspots controlled by deep-sea

circulation. *Science*, **368**, 1140–1145, https://doi.org/10.1126/science.aba5899

Koelmans, A., Kooi, M., Law, K.L. and van Sebille, E. 2017. All is not lost: deriving a top-down mass budget of plastic at sea. *Environmental Research Letters*, **12**, 114028, https://doi.org/10.1088/1748-9326/aa9500

Lebreton, L.C.M., van der Zwet, J., Damsteeg, J.-W., Slat, B., Andrady, A. and Reisser, J. 2017. River plastic emissions to the world's oceans. *Nature Communications*, **8**, https://doi.org/10.1038/ncomms15611

Li, M.Z., Prescott, R.H. and Robertson, A.G. 2019. Observations of internal tides and sediment transport processes at the head of the Logan Canyon on central Scotian Slope, eastern Canada. *Journal of Marine Systems*, **193**, 103–125, https://doi.org/10.1016/j.jmarsys.2019.02.007

Maier, K.L., Rosenberger, K.J. *et al.* 2019. Sediment and organic carbon transport and deposition driven by internal tides along Monterey Canyon, offshore California. *Deep Sea Research Part I: Oceanographic Research Papers*, **153**, https://doi.org/10.1016/j.dsr.2019.103108

Näkki, P., Setälä, O. and Lehtiniemi, M. 2017. Bioturbation transports secondary microplastics to deeper layers in soft marine sediment in the northern Baltic Sea. *Marine Pollution Bulletin*, **119**, 255–261, https://doi.org/10.1016/j.marpolbul.2017.03.065

Napper, I.E. and Thompson, R.C. 2016. Release of synthetic microplastic plastic fibres from domestic washing machines: Effects of fabric type and washing conditions. *Marine Pollution Bulletin*, **112**, 39–45, https://doi.org/10.1016/j.marpolbul.2016.09.025

Normandeau, A., Dafoe, L.T., Li, M.Z., Campbell, D.C. and Jenner, K.A. 2024. Sedimentary record of bottom currents and internal tides in a modern highstand submarine canyon head. *Sedimentology*, **71**, 1061–1083, https://doi.org/10.1111/sed.13165

Normark, W. 1970. Growth patterns of deep-sea fans. *AAPG Bulletin*, **54**, 2170–2195.

NPWS 2023. *Conservation objectives for Southern Canyons SAC [002278]. First Order Site-Specific Conservation Objectives Version 1.0*. Department of Housing, Local Government and Heritage, Dublin, https://www.npws.ie/sites/default/files/protected-sites/conservation_objectives/CO002278.pdf

Palanques, A., Puig, P., Martín, J., Durán, R., Cabrera, C. and Paradis, S. 2024. Direct and deferred sediment-transport events and seafloor disturbance induced by trawling in submarine canyons. *Science of The Total Environment*, **947**, https://doi.org/10.1016/j.scitotenv.2024.174470

Paull, C.K., Green, H.G., Ussler, W. and Mitts, P.J. 2002. Pesticides as tracers of sediment transport through Monterey Canyon. *Geo-Marine Letters*, **22**, 121–126, https://doi.org/10.1007/s00367-002-0110-1

Pierdomenico, M., Berhardt, A. *et al.* 2023. Transport and accumulation of litter in submarine canyons: a geoscience perspective. *Frontiers in Marine Science*, **10**, https://doi.org/10.3389/fmars.2023.1224859

Plastics Europe 2023. Plastics – the *fast* Facts 2023. Plastics Europe, Brussels, https://plasticseurope.org/knowledge-hub/plastics-the-fast-facts-2023/ [last accessed 24 June 2024].

Pohl, F., Eggenhuisen, J.T., Kane, I.A. and Clare, M.A. 2020. Transport and burial of microplastics in deep-marine sediments by turbidity currents. *Environmental Science & Technology*, **54**, 4180–4189, https://doi.org/10.1021/acs.est.9b07527

Rohais, S., Armitage, J.J. *et al.* 2024. A source-to-sink perspective of an anthropogenic marker: A first assessment of microplastic concentration, pathways, and accumulation across the environment. *Earth-Science Reviews*, **254**, https://doi.org/10.1016/j.earscirev.2024.104822

Talling, P.J., Cartigny, M.J.B. *et al.* 2023. Detailed monitoring reveals the nature of submarine turbidity currents. *Nature Reviews Earth & Environment*, **4**, 642–658, https://doi.org/10.1038/s43017-023-00458-1

Tarhan, L.G., Droser, M.L., Planavsky, N.J. and Johnston, D.T. 2015. Protracted development of bioturbation through the early Paleozoic Era. *Nature Geoscience*, **8**, 865–869, https://doi.org/10.1038/ngeo2537

Thompson, R.C., Olsen, Y., Mitchell, R.P., Davis, A. and Rowland, S.J. 2004. Lost at sea: where is all the plastic? *Science*, **304**, 838, https://doi.org/10.1126/science.1094559

Treignier, C., Derenne, S. and Saliot, A. 2006. Terrestrial and marine *n*-alcohol inputs and degradation processes relating to a sudden turbidity current in the Zaire canyon. *Organic Geochemistry*, **37**, 1170–1184, https://doi.org/10.1016/j.orggeochem.2006.03.010

Uddin, S., Fowler, S.W., Uddin, M.F., Behbehani, M. and Naji, A. 2021. A review of microplastic distribution in sediment profiles. *Marine Pollution Bulletin*, **163**, https://doi.org/10.1016/j.marpolbul.2021.111973

Van Cauwenberghe, L., Vanreusel, A., Mees, J. and Janssen, C.R. 2013. Microplastic pollution in deep-sea sediments. *Environmental Pollution*, **182**, 495–499, https://doi.org/10.1016/j.envpol.2013.08.013

Van Cauwenberghe, L., Devriese, L., Galgani, F., Robbens, J. and Janssen, C.R. 2015. Microplastics in sediments: a review of techniques, occurrence and effects. *Marine Environmental Research*, **111**, 5–17, https://doi.org/10.1016/j.marenvres.2015.06.007

van Haren, H., Mienis, F. and Duineveld, G. 2022. Contrasting internal tide turbulence in a tributary of the Whittard Canyon. *Continental Shelf Research*, **236**, https://doi.org/10.1016/j.csr.2022.104679

Vianello, A., Boldrin, A., Guerriero, P., Moschino, V., Rella, R. and Sturaro, A. 2013. Microplastic particles in sediments of Lagoon of Venice, Italy: First observations on occurrence, spatial patterns and identification. *Estuarine, Coastal and Shelf Science*, **130**, 54–61, https://doi.org/10.1016/j.ecss.2013.03.022

Waldschläger, K. and Schüttrumpf, H. 2020. Infiltration behavior of microplastic particles with different densities, sizes, and shapes – from glass spheres to natural sediments. *Environmental Science & Technology*, **54**, 9366–9373, https://doi.org/10.1021/acs.est.0c01722

Woodall, L.C., Sanchez-Vidal, A. *et al.* 2014. The deep sea is a major sink for microplastic debris. *Royal Society Open Science*, **1**, https://doi.org/10.1098/rsos.140317

Xue, B., Zhang, L., Li, R., Wang, Y., Guo, J., Yu, K. and Wang, S. 2020. Underestimated microplastic pollution derived from fishery activities and 'hidden' in deep sediment. *Environmental Science &Technology*, **54**, 2210–2217, https://doi.org/10.1021/acs.est.9b04850

Zhang, X., Liu, Z., Li, D., Zhao, Y. and Zhang, Y. 2024. Turbidity currents regulate the transport and settling of microplastics in a deep-sea submarine canyon. *Geology*, **52**, 646–650, https://doi.org/10.1130/G52116.1

Zhong, G. and Peng, X. 2021. Transport and accumulation of plastic litter in submarine canyons – the role of gravity flows. *Geology*, **49**, 581–586, https://doi.org/10.1130/G48536.1

Zitko, V. and Hanlon, M. 1991. Another source of pollution by plastics: Skin cleaners with plastic scrubbers. *Marine Pollution Bulletin*, **22**, 41–42, https://doi.org/10.1016/0025-326X(91)90444-W